

VOYAGER SPECTRAL OBSERVATIONS OF THE CYGNUS LOOP NEBULA, 600-1700 Å

D. E. SHEMANSKY AND B. R. SANDEL
 Lunar and Planetary Laboratory, University of Arizona

AND

A. L. BROADFOOT
 Kitt Peak National Observatory*

Received 1978 July 25; accepted 1979 January 15

ABSTRACT

Observations of the Cygnus Loop objects NGC 6995 and NGC 6992 and their near vicinity by the *Voyager 2* UV spectrometer have provided measurable emissions in the 912-1680 Å region. Emission lines in the 912-1050 Å region appear spatially correlated to the objects. The longer wavelength signal, 1200-1680 Å, shows some spatial variation comparable to recent X-ray images. In the shorter wavelength region, the estimated line positions and intensities are 940 ± 4 Å, 2 rayleighs (R), 977 ± 2 Å, 12 R, 999.6 ± 2 Å, 3.3 R, 1037.2 ± 1 Å, 29 R. We identify the feature at 977 Å with C III. The 1037 Å feature is well defined in the observed spectrum, but its identification with C II as a source is chosen from a group of unsatisfactory candidates. The brightness of these two features, along with their confinement to the optical filaments, leads to the suggestion that the emissions are associated with the relatively cool plasma. The two weaker features are tentatively identified with the O I lines at 936.0 Å and 999.6 Å. The brightest feature in the spectrum is at 1222 (+10, -2) Å, with a surface brightness ≥ 140 R measured in the direction of the objects NGC 6995 and NGC 6992. Measurable emission was obtained in the 1250-1680 Å region, but wavelength definition of features was poor owing to low counting statistics.

Subject headings: line identifications — nebulae: individual — nebulae: supernova remnants — ultraviolet: spectra

I. INTRODUCTION

The Cygnus Loop nebula has a chaotic structure that tends to make analysis of observed spectra difficult as a result of uncertainty in the contents along the line of sight. The object is generally assumed to be a supernova remnant since it lacks a known exciting star and because of other physical evidence (Parker 1967; see Chamberlain 1953). The thermal energy is consequently assumed to arise in the interaction of the expanding shell with the interstellar medium. There have been a number of reported observations in the visible and UV spectrum; Parker (1967) studied spectral lines of H α , H β , O II, O III, and N II, which suggest temperatures in the range 10^4 - 10^5 K. Later observations of soft X-rays and of the Fe XIV line suggest the inclusion of much higher temperature processes, about 3×10^6 K (Rappaport, Doxey, and Solinger 1974; Woodgate, Kirshner, and Balon 1977). The only far-ultraviolet observations (short of 3000 Å) in the literature are the Schmidt camera images obtained by Carruthers and Page (1976) during the *Apollo 16* mission. These were obtained in broadband radiation in the 1250-1600 Å range (100 rayleighs [R]) and in the 1050-1600 Å range (greater than 130 R).

* Kitt Peak National Observatory is operated by the Association of Universities for Research in Astronomy, Inc., under contract with the National Science Foundation.

We report observations of the Cygnus Loop objects NGC 6995 and NGC 6992, which are defined by bright filamentary structure in visible radiation. The observations were made with the *Voyager 2* ultraviolet spectrometer operating in the spectral range 600-1700 Å. Comparisons are made with the observations noted above. We find that there are measurable line-emission features in the spectrum. The most prominent occur at wavelengths below 1050 Å, beyond the range of the *Apollo 16* experiment.

II. INSTRUMENTATION

A full description of the *Voyager* ultraviolet spectrometer is given by Broadfoot *et al.* (1977). The instrument is an objective grating spectrometer with a one-dimensional image tube at its focal plane. It covers the wavelength range 500-1700 Å in 128 contiguous intervals. The spectrometers were designed primarily for observations of planetary atmospheres, but the field of view is narrow enough to make the instrument useful for some types of stellar observations. The field of view is 0°1 full width at half-maximum (FWHM) in the dispersive direction and 0°87 full width in the cross-dispersion direction. The spectral half-width corresponding to the dispersive field is 33 Å; the detector has a spectral sample width, or channel width, of 9.26 Å.

The detector is a photon counting system which utilizes a 128 element linear self-scanned anode array

(Reticon) (Broadfoot and Sandel 1977). The instrument is thus an imaging device. The entire spectral range of the instrument is detected simultaneously. In crude comparison with a conventional scanning spectrometer, our instrument has a factor of 128 more throughput due to the array detector. The smaller size of the detectors compared with a photomultiplier cathode provides an improvement in noise level of at least two orders of magnitude; the intrinsic noise rate is about 3×10^{-3} counts channel $^{-1}$ s $^{-1}$. Our long observing periods in spaceflight allow us to take advantage of this low noise level.

The spectrometer has no moving parts. Therefore, there are no mechanical uncertainties in the formation of the spectrum. Owing to the precise nature of the spectral line shape, wavelength determinations can be made to within ± 1 Å in cases where blending is not serious. It is important to note that precision of the instrumental transmission function is not affected by temporal variations in the source because the entire spectrum is integrated simultaneously. The theoretical shape of the transmission function and spectral dispersion have been confirmed by laboratory calibration and observations of interstellar radiation.

It is difficult to define a single dynamic range of the instrument. In some experiments we observe the Sun directly with photo event rates of 3×10^5 channel $^{-1}$ s $^{-1}$, and in other experiments we are limited only by the intrinsic detector noise of 3×10^{-3} counts channel $^{-1}$ s $^{-1}$. Within a given spectrum, we are limited by internal instrumental scattering of the incoming radiation. The internal scattering characteristics have been measured in the laboratory. Scattering matrix operators developed from the laboratory observations are used to remove the scattered components in the spectral analysis procedure. Limited experience with the matrices in observations of the interstellar medium suggest that they are accurate (Sandel, Shemansky, and Broadfoot 1979), and provide a realizable dynamic range in the vicinity of 10^4 . A description of instrument sensitivity is given by Shemansky, Sandel, and Broadfoot (1979).

III. DATA COLLECTION CONSIDERATIONS

In a typical observation sequence, the scan platform is pointed toward the target and fixed in position relative to the spacecraft. There are two motions of the spacecraft which cause the field of view to move slowly in the sky. First, the spacecraft orientation is stabilized in three axes to a tolerance (limit cycle) of $\pm 0.5^\circ$ with a cyclic period of about 1 hour. The second motion is a slower uniform drift of the mean pointing direction caused by motion of the spacecraft along its trajectory. Spectra were obtained from the instrument every 12 s and each spectrum was labeled with the instantaneous direction of the field of view to an accuracy of $\pm 0.01^\circ$. The spectra can then be readily integrated over any selected region of the celestial sphere by computer program, in order to increase statistical accuracy. Of the order of 1000

individual spectra are summed in the selected regions discussed below.

The raw signal from the spectrometer is composed of several identifiable components. The instrument-related contributions are internal scattering, discussed above, and detector noise caused by the penetration of high-energy particles. The dispersed spectrum contains emission from the foreground and the object, assuming that the object is opaque to the background. The spectral analysis follows the normal process of subtracting a normalized control spectrum which does not contain the primary object. The control spectrum ideally is obtained as close to the object as possible and contains a signal from the foreground to the object, plus a background signal. The background signal, as we indicate below, is measurable in some directions but too weak to be of significance to the quality of the spectrum as a reference for the object spectrum.

The detector background noise has a simple spectral shape and does not vary significantly during periods of normal solar activity. This component is subtracted first.

The foreground spectrum is dominated by the H $L\alpha$ line and its accompanying characteristic internal scattering pattern. Details of the nature of the spectral content have been discussed by Shemansky, Sandel, and Broadfoot (1979). The H $L\alpha$ emission arises as a result of resonance scattering of solar emission by the local interstellar medium. Its intensity changes with observational direction and with changes in solar activity; for this reason it is desirable to obtain foreground spectra as close as possible to the object of interest.

The signal defined as background emission we assume arises beyond 700 pc. The question of the accuracy of this assumption is not of practical importance to this analysis since the signal is very weak and no attempt was made to correct the control spectrum. The background is measurable with the *Voyager* UV instruments and is characterized by diffuse emission in the 900–1700 Å region with directional variability relative to 1216 Å emission (Sandel, Shemansky, and Broadfoot 1979). The maximum observed brightness at 975 Å due to the diffuse emission is only about $0.05 R \text{ Å}^{-1}$, a negligible quantity in the present analysis.

IV. OBSERVATIONS

A spatially well-defined source was readily detected in emission features in the 950–1050 Å region in the direction of NGC 6992 and NGC 6995, centered at $\alpha 313^\circ 5$, $\delta 31^\circ 7$. The observations were obtained on day 322 of 1977. About 6 hours of observation time of a total of 14 hours were obtained with the instrumental slit projected directly on the Cygnus Loop objects. The size of the source in 950–1050 Å emission was estimated to be roughly 0.5° . For this reason, our photometric results are given in terms of surface brightness, rayleighs, where $1 R = (10^8/4\pi)$ photons s $^{-1}$ cm $^{-2}$ col $^{-1}$ (see Hunten, Roach, and Chamberlain 1956).

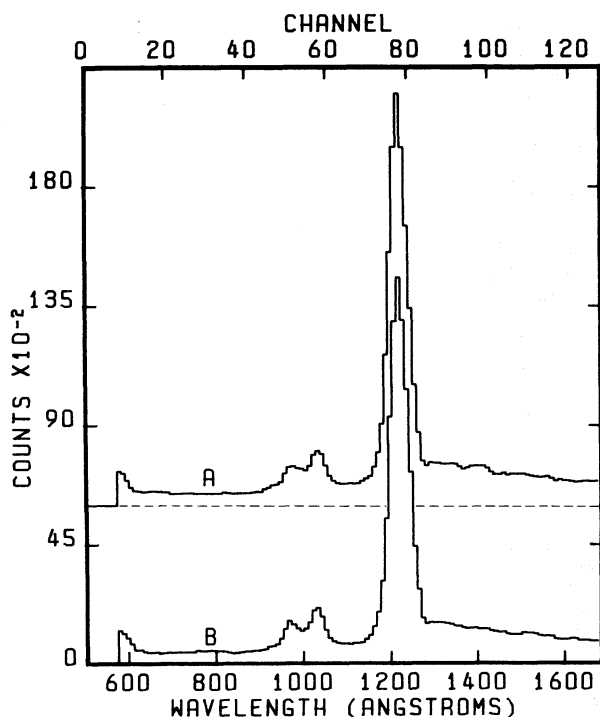


FIG. 1a, b

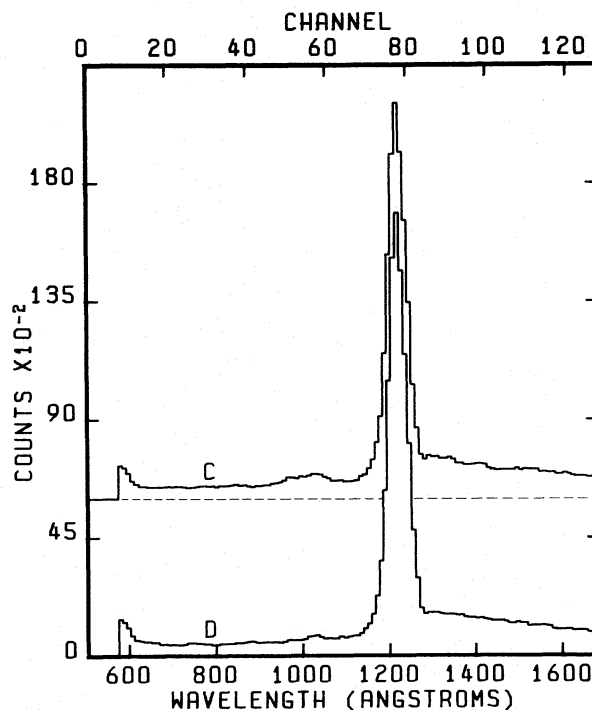


FIG. 1c, d

FIG. 1.—*Voyager 2* integrated spectra of the Cygnus Loop region. Each of the four spectra represents roughly 10^4 s of integration time. The spectra are dominated by 1216 Å solar line resonance scattering in the interstellar medium. The entrance slit size and orientation projected on the sky are shown in Fig. 2. (a) Spectrum obtained from region A of Fig. 2, which contains the objects NGC 6992 and NGC 6995. Integration time, 10836 s. (b) Spectrum obtained from region B of Fig. 2. Integration time, 9612 s. (c) Spectrum obtained inside the Loop structure, region C of Fig. 2. Integration time, 6708 s. (d) Spectrum obtained approximately 4° south of Cygnus Loop α 314 $^\circ$ 0–314 $^\circ$ 5, δ 27 $^\circ$ 2–28 $^\circ$ 4. Integration time, 11208 s.

Figures 1a, 1b, and 1c show summations of the raw data from areas A, B, and C indicated in the celestial map shown in Figure 2. Figure 2 also shows the size and orientation of the spectrometer slit; the center of the field of view was within the areas A, B, and C for the summations shown in Figure 1. The areas A, B, and C shown in Figure 2 are computer-determined boundaries, and the center of the field of view does not necessarily explore the entire indicated areas. The two locations, A and B, have the slit overlying the objects NGC 6992 and NGC 6995 and provided data with a maximum in signal strength in the 950–1050 Å spectral region. Figure 2 shows a crude outline of the filamentary structure in H α emission, taken from a Palomar Sky Survey red print. This spectral region contains the most easily recognizable signal associated with the source. Figure 1c is a summation of spectra obtained in location C approximately 0.5° inside the east edge of what is assumed to be the shock front. The 950–1050 Å signal in this spectrum is weaker, but still measurable, and is associated with the Cygnus Loop rather than foreground, according to our analysis. The field of view did not drift entirely through the eastern edge of the Cygnus Loop structure. That was unfortunate, because a spectrum just outside the eastern edge

would have given the best foreground spectrum. It was necessary to take a foreground reference spectrum from data obtained about 4 days earlier at a location roughly 4° south of the NGC 6992, NGC 6995 complex. Although this is the most appropriate spectrum we have for the foreground subtraction process, it has a shortcoming in that the observational period was somewhat shorter than the Cygnus Loop spectra. The statistical error in the difference spectrum was contributed largely by the background spectrum, Figure 1d.

We argue below that the background spectrum shown in Figure 3a can be used instead of Figure 1d. The spectrum in Figure 1d represents 3 hours of integration time in the approximate direction α 314 $^\circ$ 4, δ 27 $^\circ$ 0. Figure 3a shows a spectrum obtained about 60 days earlier with the same instrument at approximately α 324 $^\circ$, δ -23° with an integration time of 140 hours. This spectrum has been analyzed by Sandel, Shemansky, and Broadfoot (1979). The instrument spectral response is temporally stable, and the shape of the “1216 Å” feature in the interstellar-medium spectra is invariant with observational direction and time. The intensity does vary substantially. Figure 3b shows the result of subtraction of the foreground spectrum (Fig. 1d) from the spectrum of

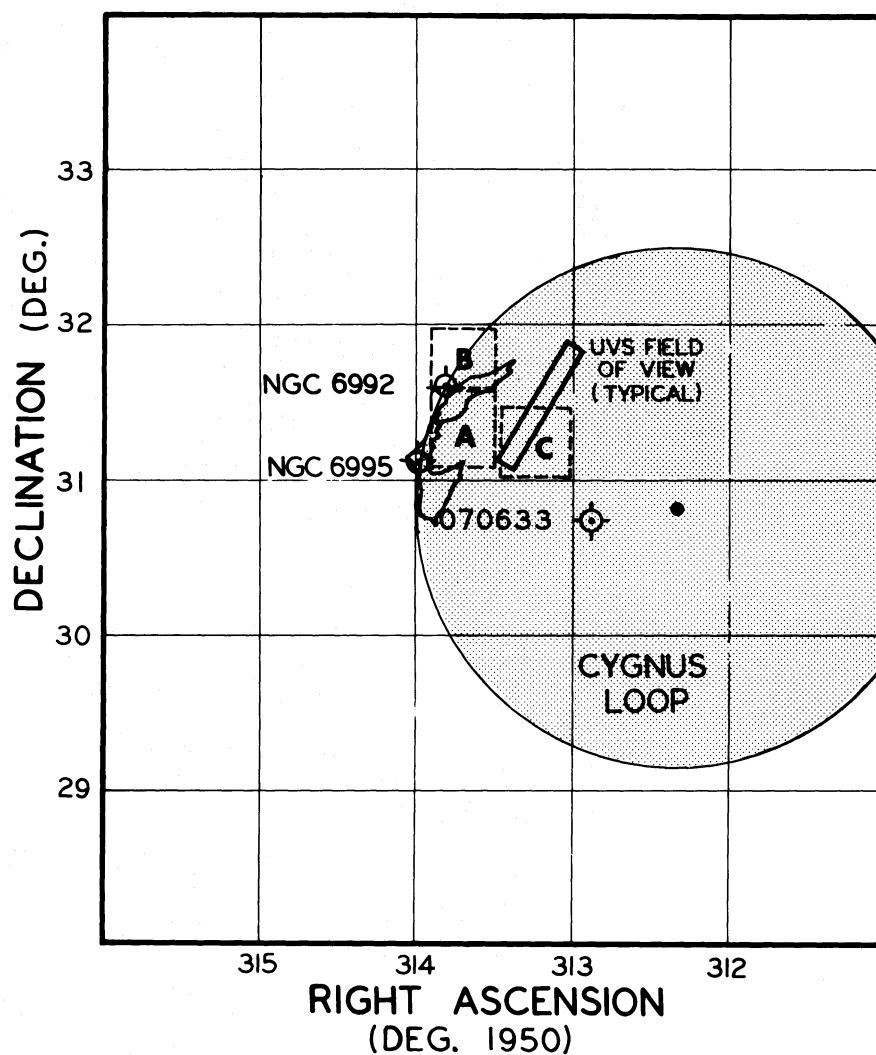


FIG. 2.—Celestial map of Cygnus Loop region. The dashed rectangles indicate the region in which the central axis of the field of view remained while the spectra of Fig. 1 were obtained. The solid rectangle illustrates the size and orientation of the projected spectrometer entrance slit. A crude outline of the filamentary structure in $H\alpha$ emission taken from a Palomar Sky Survey red print is shown in the figure along with the nominal location of NGC 6992 and NGC 6995.

Figure 3a, after normalization to the signal in the 1216 \AA feature of Figure 1d. The statistical uncertainty in the result shown in Figure 3b is due almost entirely to the Cygnus foreground spectrum; the statistical uncertainty in the peak signal of the Cygnus foreground data is roughly $\pm 1\%$, whereas the corresponding signal of Figure 3a has statistical uncertainty of $\pm 0.1\%$. There is no indication of a real difference in the spectral content in the two spectra; therefore, the spectrum in Figure 3a is used in the subtraction process in order to take advantage of its higher statistical accuracy.

Figures 4a, 4b, and 4c show the Cygnus Loop spectra, 1a, 1b, and 1c, after subtraction of the normalized foreground spectrum, Figure 3a. With this data set, we cannot normalize the spectra on the basis of integration time because the Cygnus Loop

spectra and foreground were taken from different regions of the sky. Therefore, we adjust the normalization factor iteratively to remove the 1216 \AA emission. The iteration is performed on the basis that no part of the resultant spectrum should have a statistically significant negative component after taking into account internal scattering. Subtraction is performed first, and the remaining spectrum is then corrected for instrumental artifacts and internal scattering by operating on the spectral data with an inverted "impulsive response matrix" (see Shemansky, Sandel, and Broadfoot 1979). The result is shown as the bottom curve in Figures 4a, 4b, and 4c. The same normalization was applied to the foreground spectrum, Figure 3a, for each subtraction.

Each of the difference spectra of the Cygnus Loop shows a feature just longward of 1216 \AA . We believe

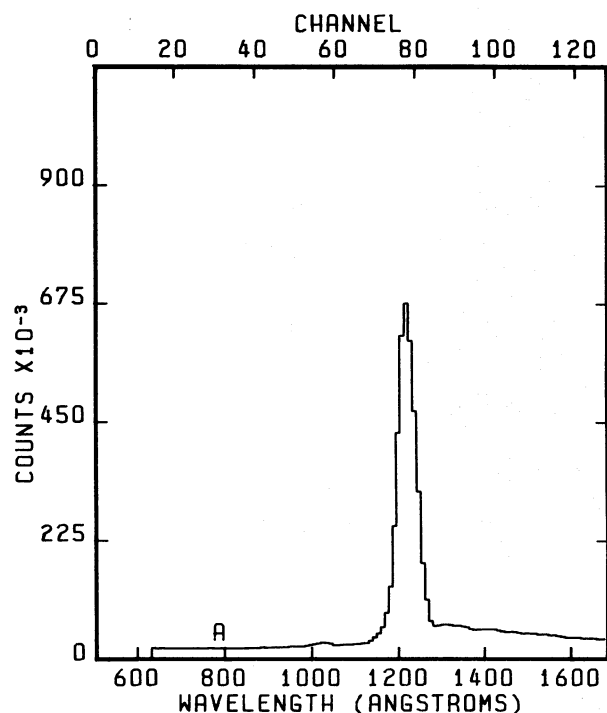


FIG. 3a

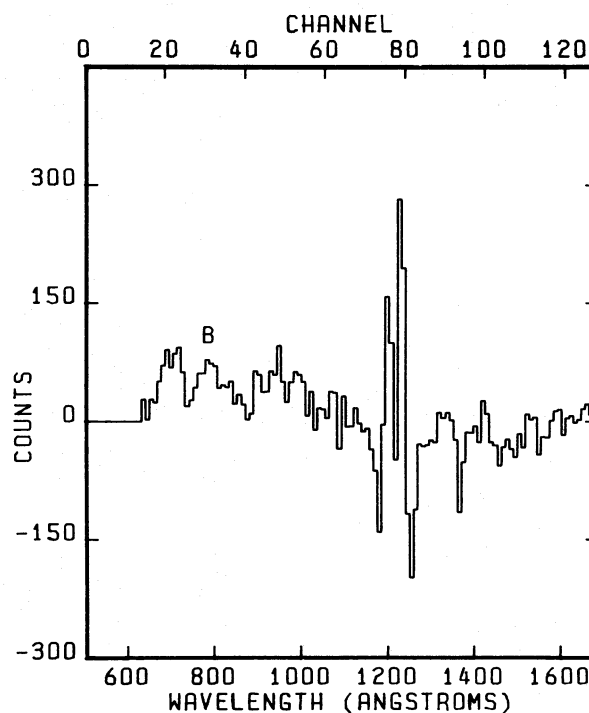


FIG. 3b

FIG. 3.—(a) Spectrum of the interstellar medium α 324°, δ -23°. Integration time, 5.011×10^6 s. According to analysis (see text) the spectrum contains detectable emission only in the He 584 and the H 1026 Å, 1216 Å lines. (b) Difference spectrum ($3a - 1d$) in which the 1216 Å feature of spectrum 3a was normalized to the magnitude of that of 1d. The slight systematic difference in the short-wavelength region could be due to difference in cosmic-ray noise levels and He 584 Å relative emission rates.

this feature to be real in spite of the large correction which was made to eliminate the foreground 1216 Å emission. We performed several tests to show that an additional emission is present. A careful comparison of the 1216 Å line shapes in Figures 1a, 1b, and 1c with 1d and 3a shows a slight excess in the channels around 80; there is no mechanism by which the line shape generated by spatially extended emission from a monochromatic source can change from one spectrum to the next. This point is illustrated by the effect of subtraction at the short wavelength side of the 1216 Å line where no excess appears. The cancellation of the short wavelength side of the 1216 Å line was within the statistical error, while the excess toward the long wavelength side persists well above the statistical limit. Figure 3b shows the effect of low statistical accuracy in the subtracted background; randomness appears on both sides of the emission line.

We have planned further observations of this object in which the variation of the spectral content will be tracked through the shock front into the adjacent region clear of the Cygnus Loop.

a) Spatial Intensity Variations

The spectral features in the 950–1050 Å region appear to be the only emissions that have a well-defined spatial association with the objects NGC 6992 and NGC 6995. The source in this spectral

region appears to be roughly 0.5 in radius approximately centered on the objects. However, we note that the field of view did not drift far enough to provide a good definition of the eastward edge of the structure. The spectral feature associated with the Cygnus Loop at 1222 (+10, -2) Å, which is by far the brightest feature in the spectrum, has no apparent direct intensity correlation with the shorter wavelength emissions. The spectrum of Figure 4c, taken about 0.5 west toward the center of the Loop, shows slightly diminished brightness in 1222 Å emission, whereas the shorter wavelength emissions are reduced by a factor of 5. The broad spectral region 1250–1680 Å also has measurable emission at each of the three spatial locations, but the total brightness does not vary substantially. Thus, the only emissions that appear to be directly associated with NGC 6992 or NGC 6995 are in the 950–1050 Å region.

b) Wavelength Analysis and Spectral Content

The spectral content and wavelength of the prominent features in the spectrum were determined with an iterative process of spectral synthesis. Figure 5 shows the observed spectrum from Figure 4a in comparison with a synthesized spectrum. In the synthesis process, the line wavelengths and intensities are estimated. The spectrum is then generated by operating on the estimated line spectrum with the

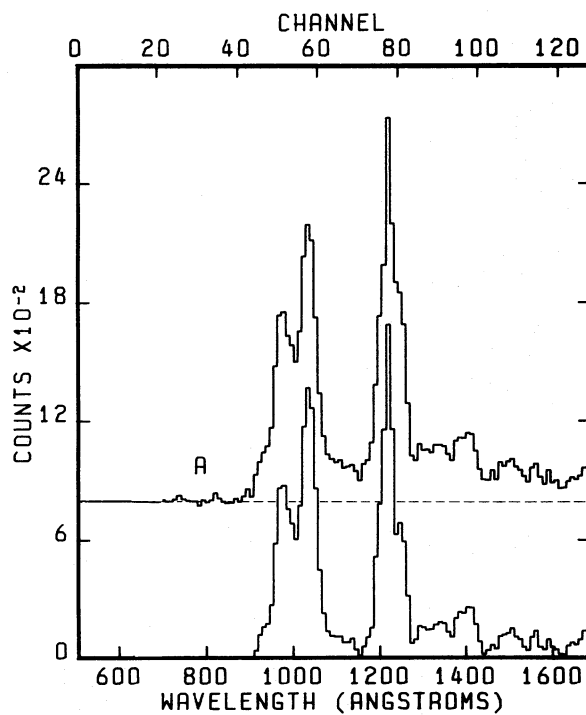


FIG. 4a

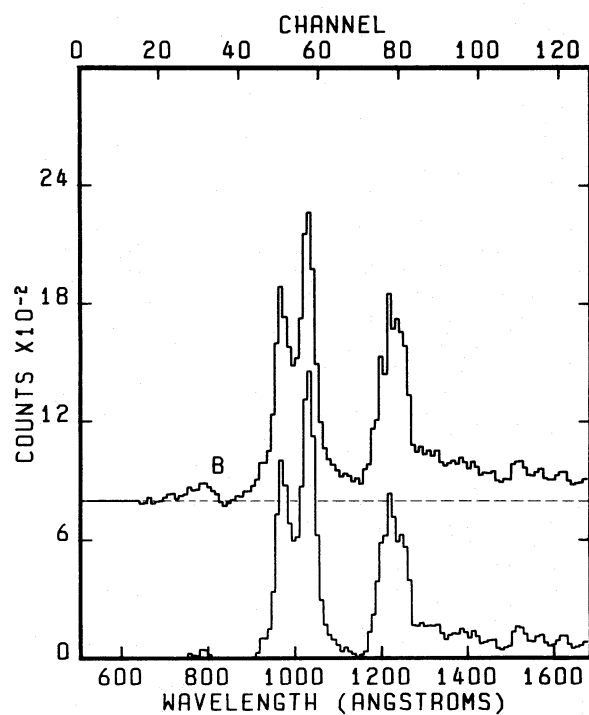


FIG. 4b

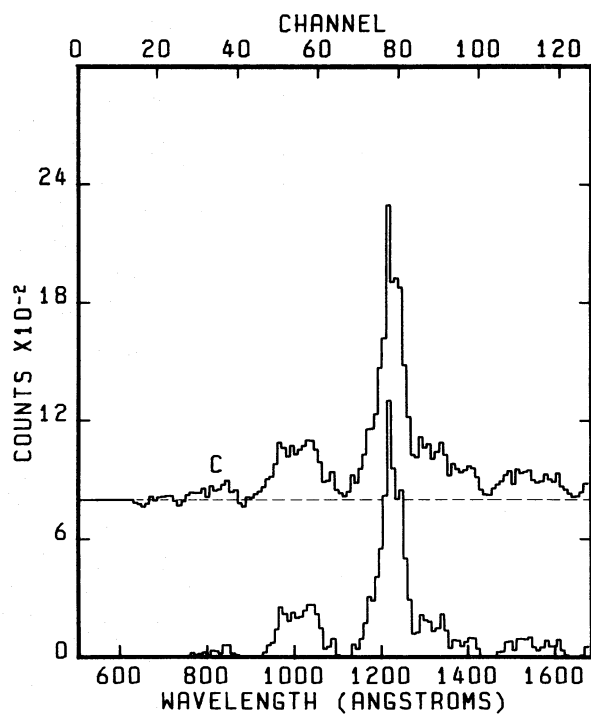


FIG. 4c

FIG. 4.—(a) The spectrum of Fig. 1a after subtraction of the foreground spectrum 3a. The lower spectrum is the result of removal of internal instrumental scattering from the upper spectrum. (b) Spectrum 1b treated in the same manner as above. (c) Spectrum 1c treated in the same manner as above.

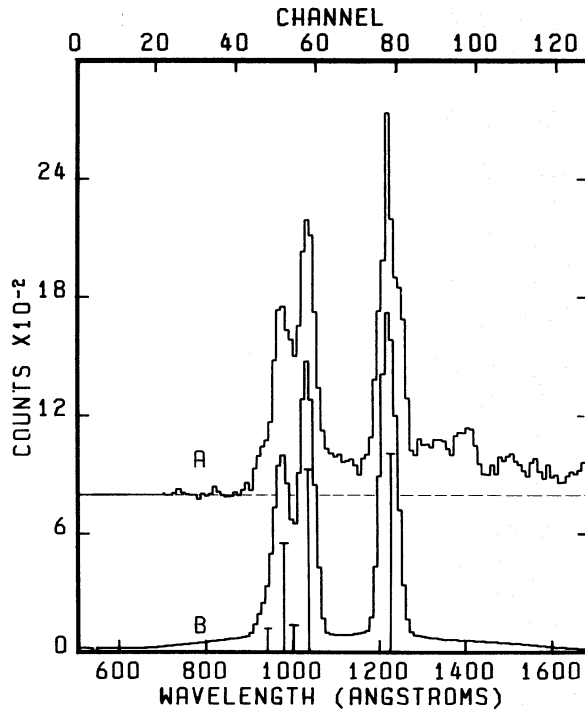


FIG. 5a, b

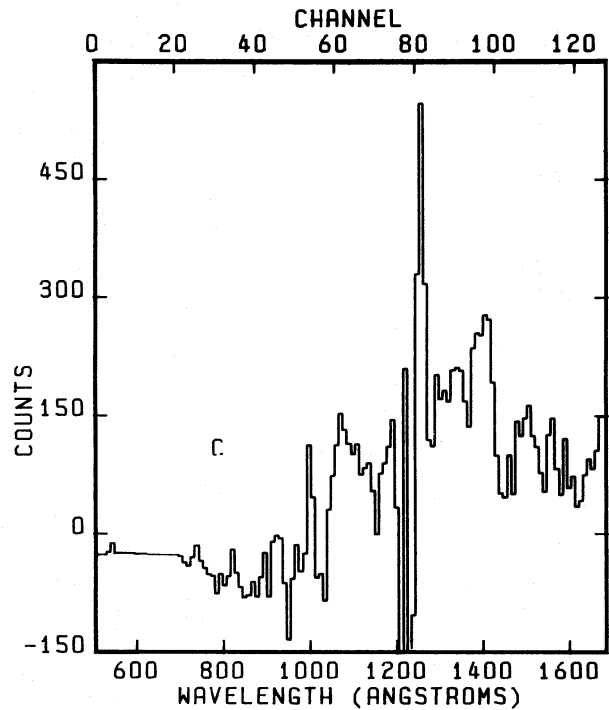


FIG. 5c

FIG. 5.—(a, b) Upper spectrum of Fig. 4a, b: synthetic spectrum containing spectral lines indicated in the figure and in Table 1. The spectrum includes predicted internal instrumental scattering. (c) Spectrum 5a after subtraction of synthetic spectrum 5b.

impulsive response matrix for the instrument; this matrix includes the instrumental line broadening, instrumental artifacts, and scattering arising from the lines themselves. The estimated wavelengths of the prominent features of the spectrum are given in Table 1. In the synthesis process, it became clear that the two prominent lines at 977 and 1037 Å could not be alone. There was a bulge on the short wavelength side of the 977 Å line, and the space between the lines was filled significantly more than predicted by a synthesis using only the two bright lines. The shapes were adjusted by including the two low-intensity lines at 940 and 999 Å. These two lines provide one solution, whereas other solutions are possible within the constraints of wavelength and intensity given in Table 1. The difference spectrum (Fig. 5a minus 5b) shown in Figure 5c indicates a satisfactory cancellation of the short-wavelength lines. There is some noise associated with the line at 1222 Å which is related to the previous subtraction of the foreground spectrum. There is an excess in emission longward of 1050 Å. There is some weak indication of the presence of features in the vicinity of 1337, 1411, and 1550 Å.

c) Absolute Brightness

The column brightness of the features of the spectra are given in Table 1. These data are based on laboratory calibration using calibrated channeltron detectors as absolute monitors. The detector calibrations are

traceable to NBS standard photodiodes. The only other data available for comparison are the Carruthers and Page (1976) results, included in Table 1. There is good agreement in respect to the total brightness in the 1250–1680 Å region. Carruthers and Page provide only an upper limit to the brightness in the 1050–1600 Å region. Figure 6 shows the spectrum of Figure 4a on an absolute-brightness scale.

V. DISCUSSION

We have already noted that the source of the radiation in the 912–1050 Å region is localized near the objects NGC 6995 and NGC 6992, which are defined

TABLE 1
SPECTRAL CONTENT OF CYGNUS UV OBSERVATIONS

$\lambda(\text{\AA})$	I_1^*	I_2	I_3	I_4
940 ± 4	2	1.4
977 ± 2	12	14	4	...
999.6 ± 4	3.3
1037.2 ± 1	29	29	5.7	...
$1222 (+10, -2)$	138	71	110	...
1050–1680.....	254	185	184	> 130
1250–1680.....	116	114	74	100

* Brightness in rayleighs: (1) Fig. 4a, α 313.7, δ 31.35 (1950); (2) Fig. 4b, α 313.7, δ 31.8; (3) Fig. 4c, α 313.2, δ 31.25; (4) Carruthers and Page 1976, maximum brightness on NGC 6992, α 313:83, δ 31:6.

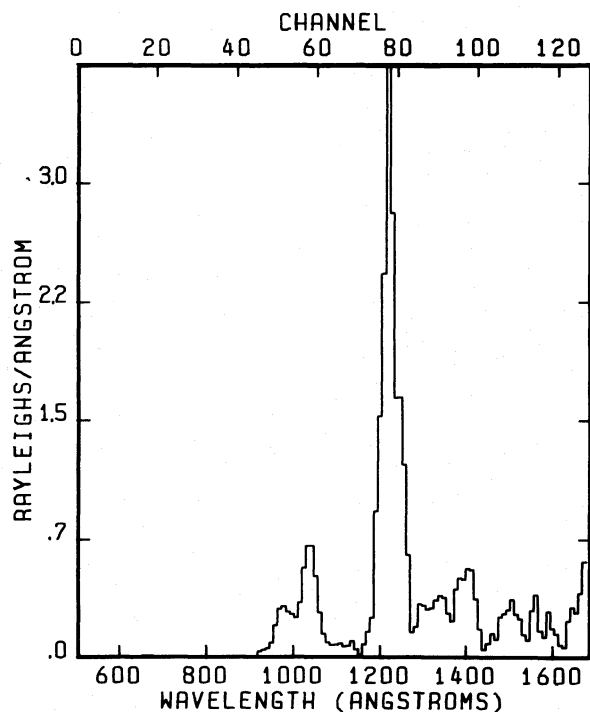


FIG. 6.—Spectrum of Fig. 4a on an absolute brightness scale.

by bright filamentary structures in visible wavelengths such as $H\alpha$ (Parker 1967). In contrast, the signal in the 1200–1680 Å region shows significantly less spatial variation over the observed portions of the Loop. We therefore discuss these spectral regions separately.

a) The 912–1050 Å Region

The fact that the emission is bright along with the spatial confinement suggests that it is associated with the cooler filamentary regions. Line identifications and measured relative intensities discussed below indicate that the observed emission does in fact originate in the cool post-shock regions of the Loop structure.

Other observations of the filaments (Parker 1967; Cox 1972) suggest an inhomogeneous structure with temperatures ranging between 10^4 and 3×10^5 K. As Parker (1967) has pointed out, this makes interpretation difficult since one is never sure that the observations arise from a single filamentary component. The present observations certainly suffer from this problem. Using Doppler velocities inferred from optical observations together with models of the heating due to a shock front moving through the interstellar medium leads to an inference of the temperature. Along this line, Parker (1967) suggested that the filaments were the result of a shock front expanding at 100 km s^{-1} through discrete clouds in the interstellar medium. The heated gas produces a spectrum characterized by a mixture of collisional and radiative ionization-excitation. This general

description is supported by the later measurements by Miller (1974) and the shock wave calculations of Cox (1972).

Recent observations which indicate a much higher shock velocity, about 400 km s^{-1} , require a somewhat different process. It has been proposed that the denser regions of the interstellar medium may propagate a slower shock wave (about 100 km s^{-1}) on impact by the primary shock wave. Thus the filaments are represented as the primary phenomenon of collisional excitation (McKee and Cowie 1975). Observations of the spatial distribution of the [Ar iv] 4740 Å line by Woodgate, Kirshner, and Balon (1977), on the other hand, have raised the possibility that the filaments may be formed by radiative cooling instabilities. Whatever the case may be it appears that an emission sharply confined to the filamentary objects is not likely to be characterized by ionization temperatures much greater than 10^5 K. This view is compatible with the ionization temperatures of 10^4 – 10^5 K inferred from the lower limit of the intensity ratio $I(\text{C III } 977)/I(\text{C IV } 1550)$.

The most easily identified line is the C III 977 Å transition corresponding to the second most prominent feature in this wavelength region. A list of species considered as possible sources of the observed emission is given in Table 2. This list is based mostly on wavelength correlation with the observed lines. The only other potentially measurable feature near this wavelength is He II at 972 Å. The relative strengths of Osterbrock's (1963) recombination coefficients indicate that the 972 Å transition should be too weak to measure since the He II recombination line at 1640 Å is not measurable in our spectra. Our observations indicate that the ratio $I(\text{C III } 977)/I(\text{C IV } 1550) > 1$ in the optical filaments, and could be as large as 10 if we apply the standard extinction curve. This implies that the source must be dominated by relatively cool gas (10^4 – 10^5 K) (see Cox and Daltabuit 1971; see also Table 4).

Possible candidates for the line having the most accurately determined wavelength, 1037.2 Å, are C II, N IV, and O VI (see Table 2). We eliminate O VI on observational grounds. First, there is no evidence for a line near the location of the brighter O VI multiplet component at 1031.9 Å, as indicated by the synthesized spectrum shown in Figure 5. This difficulty would be removed if a species other than O VI could absorb the 1031.9 Å line in the intervening medium, but a search revealed no such species. A ground-state connected line in HD [Ly(6, 0)R(0)] is in near coincidence with the O VI 1037.6 Å component, but there is no evidence for measurable amounts of H_2 in the direction of Cygnus Loop. Second, the observed emission is confined to the cool optical filaments, whereas O VI is associated with higher temperature regions, $\geq 4 \times 10^5$ K, that are not so localized (Kirshner and Taylor 1976; Woodgate, Kirshner, and Balon 1977). The N IV line at 1036.2 Å is a possibility that cannot be entirely eliminated. However, the excitation probability of the excited state is likely to be small since it does not connect to the ground state.

TABLE 2
UV EMISSION LINES

Observation λ (Å)	$I_1(R)$	Species
940 \pm 4.....	2	949.2,* 958.7* He II; 948.3,* 955.3* N IV; 936.0* O I
977 \pm 2.....	12	972.1* He II; 977.0 C III
999.6 \pm 4.....	3.3	992.4* He II; 989.8, 991.5, 991.6 N III; 999.5* O I
1037.2 \pm 1.....	29	1036.3, 1037.0 C II; 1036.16* N IV; 1031.91, 1037.61 O VI
1222 (+10, -2).....	138	1238.8, 1242.8 N V; 1226.7,*† 1227.4,*† 1233.4,*† 1234.1*† [S II]; 1195, 1260, 1264, 1265 Si II; 1206 Si III; 1231.7*† [N I]
1250-1680.....	116	1640.5* He II; 1660.8, 1666.2 O III; 1406† [O IV]; 1334.53, 1335.66, 1335.71 C II; 1550 C IV; 1488.1 N IV; 1371.3 O V; 1304, 1309, 1527, 1533 Si II; 1394, 1403 Si IV; 1609† [Ne IV]; 1575† [Ne V]

* Not ground-state connected.

† Forbidden or low-probability transition.

The most probable dominant emitter at 1037 Å is C II at 1037.0 Å and 1036.3 Å. This conclusion is based on the characteristic temperature of the emitter and the fact that the intensity implies a reasonable density in interstellar clouds where the emission originates. However, a serious difficulty with this identification is an accompanying C II emission at 1335 Å that does not appear in our spectra with the expected relative brightness.

To illustrate this difficulty, we have calculated line emissions from a low-density plasma using the emission coefficients and collision strengths given by Osterbrock (1963), and results of calculations of ionization equilibrium in a gas with electrons as the ionizing agent by Cox and Tucker (1969). The emission quantities have been calculated from the point of view of establishing a plausible excitation regime rather than as a detailed analysis. Consequently, the numbers are approximate and the list of line emitters is not comprehensive. Table 3 shows the resulting brightness in rayleighs for two source temperatures, 3.2×10^4 K and 1.5×10^5 K. The gas is in the solar abundance distribution, with the hydrogen abundance (η_H) chosen at $\eta_H = 10^{20} \text{ cm}^{-2}$, and electron density $N_e \sim 100 \text{ cm}^{-3}$.

The calculation predicts that the C II transition at 1336 Å will be stronger than the C II line at 1037 Å. This point is illustrated in Figure 7, which shows the relative count rates that the 3.2×10^4 K emission lines would produce in the *Voyager* instrument. Other significant differences are apparent in comparison with Figure 4. Recent estimates of oscillator strengths reduce the expected relative emission rates $I(\text{C II } 1336)/I(\text{C II } 1036)$ in Table 3 by a factor of about 5 (Morton and Smith 1973; Morton 1978). In spite of this reduction, the observed 1037 Å relative emission rate is far too bright to agree with the model. Differential absorption in the intervening medium could not change the expected ratio (see Morton 1978) since the new absorption oscillator strengths for the two multiplets are very nearly equal. Although extinction is not severe in the direction of Cygnus Loop, one expects 2.3 mag at 1037 Å and 0.35 mag at 1500 Å from the standard extinction curve given by Bless and Savage (1972). We estimate an upper limit of about

TABLE 3
CALCULATED RELATIVE EMISSION RATES
FROM A LOW-DENSITY PLASMA IN
IONIZATION EQUILIBRIUM

Species	Wavelength (Å)	Photon Rate
$T = 3.2 \times 10^4 \text{ K}^*$		
N II.....	916	30
C III.....	977	17
N III.....	991	0.9
S III.....	1015	0.7
S III.....	1021	0.9
C II.....	1037	62
S III.....	1077	0.05
N II.....	1084	109
S III.....	1194	2.5
S III.....	1202	2.5
Si III.....	1206	496
[S II].....	1234	1.2
C II.....	1336	818
$T = 1.5 \times 10^5 \text{ K}^*$		
S VI.....	933, 944	6.7
He II.....	949	0.8
He II.....	958	1.4
C III.....	977	430
He II.....	992	2.7
S III.....	1015	8.3
S IV.....	1063, 1073	48
S III.....	1077	0.7
S III.....	1194	14
S V.....	1199	1.8
S III.....	1202	21
[S II].....	1234	0.08
N V.....	1239, 1243	8
S IV.....	1385, 1392	25
[O IV].....	1402, 1412	685
S IV.....	1404, 1410	12
N IV.....	1488	37
C IV.....	1548, 1551	578
He II.....	1640	522

* Collision strengths from Osterbrock 1963. Ionization equilibrium distribution from Cox and Tucker 1969.

† Emission rates may be taken as lower limit surface brightness in rayleighs at the source about $313^{\circ}9 \alpha$, $31^{\circ}3 \delta$ (see text, Figs. 7 and 8).

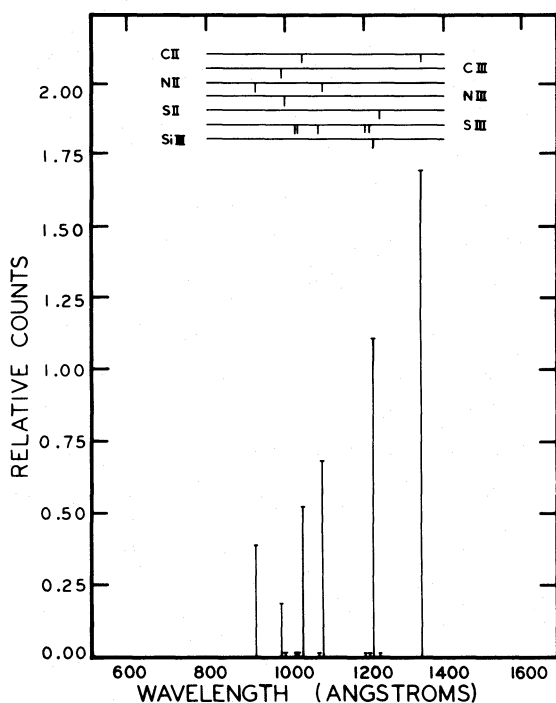


FIG. 7.—Predicted relative count rates in the *Voyager* UV instrument due to line emission in an optically thin plasma in collisional equilibrium (Table 3) at 3.2×10^4 K.

10 R for radiation at 1336 Å (see Fig. 6), placing an upper limit of 0.3 on the observed intensity ratio $I(\text{C II } 1336)/I(\text{C II } 1036)$ in the filaments. This may be compared with the predicted ratio of 13 (Table 3) or about 2.6 using Morton's oscillator strengths.

Other lines that are too bright relative to C II 1037 Å in the collisional equilibrium model at 3×10^4 K are the Si III 1206 Å and N II 1084 Å lines (see Table 3 and Table 4, col. 4). In the case of N II this could be explained only by an uncertainty in the oscillator strength of the 1084 Å transition. The lack of a measurable 1206 Å feature in the observed spectra is more easily explained by a slightly lower temperature (see Cox and Tucker 1969) and/or differential absorption in the intervening medium (see Table 4). Thus if we accept the recent oscillator strengths the identification of the 1037 Å feature with the C II transition is incompatible with the collisional ionization equilibrium model unless an additional selective excitation or extinction mechanism is introduced. Some other as yet unidentified transition at 1037 Å is a possibility as an additional contributor, since Morton (1978) indicates the presence of an unidentified absorption line at 1036.5 Å in the interstellar medium.

The two other weak lines required to produce a satisfactory synthesis of the observed 912–1050 Å spectrum could be the O I 936.0 Å and 999.5 Å lines. Both transitions are classically allowed, but are not connected to the ground state. It is not certain that all of the emissions within the 912–1050 Å region closely

follow the obvious variations in the major emitters at 977 and 1037 Å, but the shape of the spectrum inside the Loop (Fig. 4c) does not appear to deviate beyond statistical uncertainty from the measurements made while pointed directly at the filaments, although the brightness variation is a factor of 5.

Quantitative comparison of our data at short wavelengths with other measurements at longer wavelengths, assuming that our line identifications are correct, does not introduce any serious conflicts with our suggestion that the observed emissions are dominantly due to low temperature post-shock processes. Most of the quantities relevant to this discussion are given in Table 4. Observations of the very bright [O II] 3727 Å lines (Miller 1974; Table 4) indicate that the C III 977 Å effective radiative cooling coefficient ($P/N_e N_H$) must be determined on the cool side of the C III radiative cooling curve (see Cox and Daltabuit 1971). We believe that this conclusion holds in spite of the uncertainties due to extinction and differences in fields of view of Miller's and our instruments. As shown in Table 4, the abundance product $IN_e N_H$, estimated from the three transitions C III 977 Å, C II 1037 Å, and [O II] 3727 Å, differs by factors of about 3 or less for a shock temperature of 3×10^4 K. Note that if we take the Cox (1972) shock-wave mechanism as a model, the values of $IN_e N_H$ are increased by a factor of about 2 if the source of the observed emissions is in the post-shock cooling region where radiative cooling efficiencies are reduced.

These calculations are based on an assumed post-shock ionization equilibrium. More recent interstellar shock calculations (Shull and McKee 1979; Raymond 1979) relax the ionization equilibrium assumption and take radiative transfer effects into account. The Shull and McKee (1979) work in particular is the only self-consistent calculation to the extent that the ionization state of the pre-shock gas is determined by the calculated transfer of EUV radiation from the shock region. There are some quantitative differences between the models, at least partly due to differences in the preshock ionization state (Shull and McKee 1979). However, these recent model calculations do not change our suggestion that the observed 912–1050 Å radiation originates in the cool postshock gas. Comparison of the observed intensity ratios discussed above with the new models indicates shock velocities in the range 70–100 km s⁻¹, and temperatures in the range 7×10^4 K to 1.5×10^5 K. A more detailed examination of the models in light of the present observations is certainly in order, but beyond the scope of the present paper.

b) The 1200–1680 Å Region

The most striking characteristic of the radiation in this range is the spatial uniformity of its intensity compared to the signal in the 912–1050 Å region (see Figs. 4a, 4b, and 4c). The only well-defined feature in this region of the spectrum is at about 1222 Å. The features at longer wavelengths (greater than 1250 Å) are ill-defined because of the lower sensitivity of the

TABLE 4
COMPARATIVE QUANTITIES BASED ON OBSERVED EMISSIONS

Species/ λ (Å) (1)	σ (cm ²) (2)	$P/N_e N_H$ (ergs cm ³ s ⁻¹) (3)	$I(R/E)$ (4)	$IN_e N_H$ (cm ⁻⁶) (5)	N_e (cm ⁻³) (6)	τ (7)	$I'(R)$ (8)	N/N_0 (9)
C III: ¹ S- ¹ P ^o (977.0).....	2.4-13*	1.5-22 ^a 1-24 ^b	126 ^a 2.6-5	... 2.6 + 21 ^a	18 ^a 103 ^b	4 + 6 ^a 8 + 5 ^b	17
C II: ² P ^o - ² S (1037.0).....	1.8-14	1.9-24 ^b 5.3-24 ^d	241 ^a 9.5-5	2.4 + 21 ^a 8.6 + 20 ^c	25 ^a 140 ^b	5 + 5 ^a 8 + 4 ^b	62
N II: ³ P- ³ D ^o (1084).....	8-14	< 2 ^b < 3-6	109 ...	> 2-3 ...
Si III: ¹ S- ¹ P ^o (1206.5).....	1-12	< 25 ^b < 3.3-5	496 ...	> 7-4 ...
C II: ² P ^o - ² D (1336).....	9-14	3.7-23 ^a 2-23 ^b	< 10 ^b < 1.2-5	818 ...	> 1-3 ...
[O II]: ⁴ S ^o - ² D ^o (3727).....	~5-25	3.9-23 ^a 1.5-23 ^c	3400 ^c 1.4-3	4.5 + 20 ^b 1.2 + 21 ^b	21 ^a /120 ^b 34 ^a /197 ^b	1 - 5 ^a 3 - 6 ^b

* 2.4×10^{-13} .

NOTES TO TABLE 4

COL. (2).—Doppler line-center cross section, $T = 10^4$ K. More recent measurements indicate that the C II 1037 Å and 1336 Å values should be 5×10^{-14} cm² and 6×10^{-14} cm², respectively.

COL. (3).—Radiative cooling coefficient: ^(a) Peak value, from Cox and Daltabuit (1971); ^(a) $T = 3.2 \times 10^4$ K; ^(c) Mean value, from Cox (1972) shock-wave configuration; ^(d) Using the oscillator strength from Morton (1978).

COL. (4).—Estimated column brightness in rayleighs and in ergs cm⁻² s⁻¹ sr⁻¹: ^(a) Estimated source brightness assuming a standard extinction curve; see Table 1; ^(b) Observed brightness upper limit; ^(c) Miller (1974) estimated source brightness.

COL. (5).—Abundance product, $IN_e N_H$, where l is mean path length. The quantities ^(b) contain a number of uncertainties with respect to comparison with the quantities ^(a), including widely differing instrumental fields of view, and uncertainty in UV extinction; ^(c) corresponds to the radiative cooling coefficient given in col. 2^(a) above.

COL. (6).—Estimated number density $N_e = N_H$: ^(a) Assuming $l = 0.3$ pc; ^(b) Assuming $l = 10^{-2}$ pc.

COL. (7).—Optical depth: ^(a) $l = 0.3$ pc; ^(b) $l = 10^{-2}$ pc.

COL. (8).—Predicted brightness from Table 3.

COL. (9).—Number densities of ion (10^4 K) relative to parent neutrals in intervening medium required to reduce predicted emissions to the observed upper limits. An abundance $IN_H = 2.4 \times 10^{20}$ cm⁻² in the intervening medium was assumed with species in the solar abundance ratio.

instrument as we noted above. The 1222 Å feature may show weak variation in intensity relative to the 1250–1680 Å signal (Table 1), but confirmation of this with further observations is necessary. This feature shows qualitative agreement with the spatial distribution in the 1250–1600 Å images obtained by Carruthers and Page (1976), and quantitative agreement with X-ray images (Rappaport *et al.* 1979) obtained with a spatial resolution similar to the *Voyager* instrument.

The uniformity of the spatial distribution of intensity in this wavelength region raises the possibility that the source may be in the higher temperature regions of the shock front. However, there is a difficulty in making this interpretation since the bright feature at 1222 Å (possibly 200 R) would demand a very high radiative cooling coefficient for whatever species is involved. Table 3 and Figure 8 show the expected line structure for a temperature of 1.5×10^5 K, using the Cox and Tucker (1969) ionization equilibrium calculation, without taking extinction into account. Although most of the transitions connect to

the ground state, the predicted emissions in the vicinity of 1200 Å are relatively weak, and there is no hint of a sufficiently intense emission near 1222 Å.

Another possibility is that the 1222 Å radiation may be associated with the more centrally located supernova ejecta where one can expect enhanced populations of the heavier elements (Chevalier 1977). However, there appears to be no well established evidence relating observed emission to the ejecta (see McKee and Cowie 1975; Rappaport *et al.* 1979). In particular, X-ray emission seems to have a weak correlation with the optical emission and is not necessarily associated with the interior (Rappaport *et al.* 1973; Rappaport *et al.* 1979).

The upper limit to the brightness of individual line features in the 1250–1680 Å region is about 10 R . As we have noted above, there is some weak indication of the presence of lines in the vicinity of 1337, 1411, and 1550 Å, perhaps owing to emission from C III, O IV, S IV, N IV, and C IV (see Tables 2 and 3, and Fig. 9). If we use the measured intensities of the [O II] lines at 3727 Å as a reference, the Cox (1972)

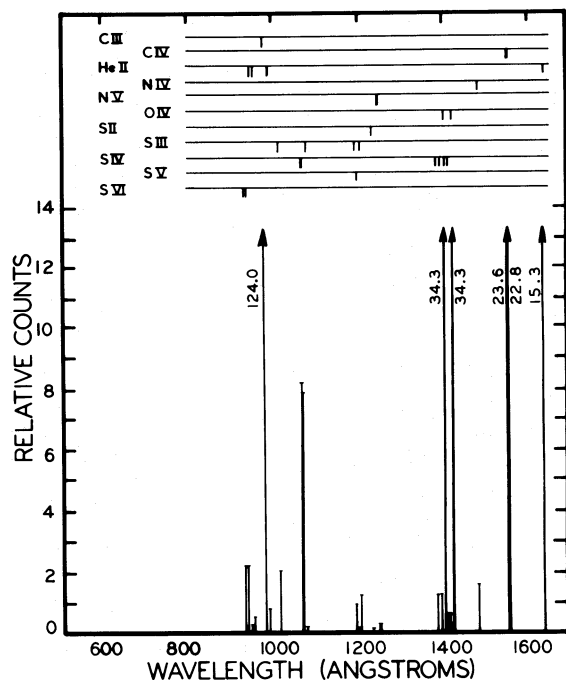


FIG. 8.—Predicted relative count rates in the *Voyager* UV instrument due to line emission in an optically thin plasma in collisional equilibrium (Table 3) at 1.5×10^6 K.

calculations would predict about $10 R$ at the source for the forbidden [Ne iv] and [Ne v] lines at 1609 and 1575 Å, with a shock propagation velocity of 140 km s^{-1} . Assuming weak extinction, the present upper limit of $10 R$ indicates a lower temperature and hence a lower propagation velocity. We have not examined the more recent shock models in sufficient detail to determine compatibility with the Cox (1972) calculations in this case.

c) UV Continuum

We obtain no evidence for continuum radiation in the observed spectral region. However, the subtraction process in which the foreground spectrum was removed tends to overestimate the magnitude of the foreground. A more refined analysis of the data could change this conclusion. Miller (1974) claims to have observed continuum radiation in the visible and near-ultraviolet region which may be at least partly due to recombination into the Balmer and Paschen series. We can place a crude upper limit of about $0.1 R \text{ Å}^{-1}$ at 1100 Å in our spectra. This would not contradict Miller's (1974) estimate of $0.5 R \text{ Å}^{-1}$ at the edge of the Balmer continuum, if one introduces a moderate amount of extinction.

VI. CONCLUSIONS

We have obtained spectra of the Cygnus Loop on and in the near vicinity of NGC 6992 and NGC 6995

in 600–1680 Å radiation. An important characteristic of the observed spectra is the spatial distribution of the emitters. Measurable emission in the 912–1050 Å region is sharply confined to the location of the optical filaments. The emissions in the 1200–1680 Å region have a less pronounced variation, a moderate decline 0.5 westward of the filaments toward the center of the Loop.

It is suggested that the radiation in the 912–1050 Å region is associated with the cooler post-shock regions. The most likely emitters in this region have been identified as 1037 Å C II, 977 Å C III, 999.5 Å O I, and 936 Å O I, based on spectral analysis and some necessary reference to physical models. The identification of the 977 Å feature with the C III transition is well established. The other identifications are less certain. There is an unresolved difficulty in attributing the bright 1037 Å feature to the C II transition. Recent absorption measurements (Morton 1978) indicate the C II 1336 Å multiplet should be brighter than the 1037 Å transition by a factor of about 2.6, whereas the observed upper limit for this ratio is 0.3. Nevertheless, other known emitters near 1037 Å appear to be more improbable than the C II transition. The feature identified as C III 977 Å emanating from the optical filaments has a relative brightness suggesting a cool post-shock source (see Table 4). The more recent shock-wave calculations do not change this conclusion. However, detailed comparisons with the new models (Shull and McKee 1979; Raymond 1979) have not yet been made. The observations of the optical filaments do not correspond to any single model condition, but shock velocities in the range $70\text{--}100 \text{ km s}^{-1}$ are indicated in the crude comparisons we have made.

The 1200–1680 Å signal is not spatially correlated with the shorter-wavelength radiation. The decrease in the long-wavelength signal from the edge of the Loop structure toward the center is more similar to the spatial structure in the recent Rappaport *et al.* (1979) X-ray images. A somewhat disconcerting aspect of the longer-wavelength data is the brightness of the 1222 Å feature. The feature is unavoidably present in spite of the fact that it is entangled with the 1216 Å foreground emission. A plausible explanation may be forbidden-line emission, possibly 1227 Å [S II], from much denser regions of the Loop structure. The excitation efficiency of the H⁻ transition at 1222 Å (cf. Drake 1973) should be examined to determine whether H⁻ may account for or contribute to the emission.

The present analysis has revealed no measurable continuum in the UV region. We place a rough upper limit of $0.1 R \text{ Å}^{-1}$ at 1100 Å, or $1.4 \times 10^{-7} \text{ ergs cm}^{-2} \text{ s}^{-1} \text{ Å}^{-1} \text{ sr}^{-1}$ for the continuum differential brightness.

We acknowledge useful discussions with and comments by J. M. Shull, J. C. Raymond, R. A. Chevalier, and J. C. McConnell.

This work was supported by the Jet Propulsion Laboratory, California Institute of Technology, under NASA contract NAS 7-100.

REFERENCES

- Bless, R. C., and Savage, B. D. 1972, *Ap. J.*, **171**, 293.
 Broadfoot, A. L., and Sandel, B. R. 1977, *Appl. Opt.*, **16**, 1533.
 Broadfoot, A. L., et al. 1977, *Space Sci. Rev.*, **21**, 183.
 Carruthers, G. R., and Page, T. 1976, *Ap. J.*, **205**, 397.
 Chamberlain, J. W. 1953, *Ap. J.*, **117**, 399.
 Chevalier, R. A. 1977, *Ann. Rev. Astr. Ap.*, **15**, 175.
 Cox, D. P. 1972, *Ap. J.*, **178**, 143.
 Cox, D. P., and Daltabuit, E. 1971, *Ap. J.*, **167**, 113.
 Cox, D. P., and Tucker, W. H. 1969, *Ap. J.*, **157**, 1157.
 Drake, G. W. F. 1973, *Ap. J.*, **184**, 145.
 Hunten, D. M., Roach, F. E., and Chamberlain, J. W. 1956, *J. Atm. Terr. Phys.*, **8**, 345.
 Kirshner, R. P., and Taylor, K. 1976, *Ap. J. (Letters)*, **208**, L83.
 McKee, C. F., and Cowie, L. L. 1975, *Ap. J.*, **195**, 715.
 Miller, J. S. 1974, *Ap. J.*, **189**, 239.
 Morton, D. C. 1978, *Ap. J.*, **222**, 863.
 Morton, D. C., and Smith, W. H. 1973, *Ap. J. Suppl.*, **26**, 333.
 Osterbrock, D. E. 1963, *Planet. Space Sci.*, **11**, 621.
 Parker, R. A. R. 1967, *Ap. J.*, **149**, 363.
 Rappaport, S., Cash, W., Doxey, R., Moore, G., Borken, R. 1973, *Ap. J. (Letters)*, **186**, L115.
 Rappaport, S., Doxey, R., and Solinger, A. 1974, *Ap. J.*, **194**, 329.
 Rappaport, S., Petre, R., Kayat, M., Evans, K., Smith, G., and Levine, A. 1979, *Ap. J.*, **227**, 285.
 Raymond, J. C. 1979, *Ap. J. Suppl.*, **39**, 1.
 Sandel, B. R., Shemansky, D. E., and Broadfoot, A. L. 1979, *Ap. J.*, **227**, 808.
 Shemansky, D. E., Sandel, B. R., and Broadfoot, A. L. 1979, *J. Geophys. Res.*, **84**, 139.
 Shull, J. M., and McKee, C. F. 1979, *Ap. J.*, **227**, 131.
 Woodgate, B. E., Kirshner, R. P., and Balon, R. J. 1977, *Ap. J. (Letters)*, **218**, L129.

A. L. BROADFOOT: Kitt Peak National Observatory, P.O. Box 26732, Tucson, AZ 85726.

B. R. SANDEL and D. E. SHEMANSKY: Voyager Program, 3625 East Ajo Way, Tucson, AZ 85713.